2D Materials

PAPER

RECEIVED
9 January 2017

REVISED
5 April 2017

ACCEPTED FOR PUBLICATION
6 April 2017

PUBLISHED
28 April 2017

Highly-ordered wide bandgap materials for quantized anomalous Hall and magnetoelectric effects

M M Otrokov[1,2,3,4], T V Menshchikova[2], M G Vergniory[1,5], I P Rusinov[2], A Yu Vyazovskaya[2], Yu M Koroteev[6,2], G Bihlmayer[7], A Ernst[8,9], P M Echenique[1,4], A Arnau[1,4] and E V Chulkov[1,3,4]

1 Donostia International Physics Center (DIPC), 20018 San Sebastián/Donostia, Spain
2 Tomsk State University, 634050 Tomsk, Russia
3 Saint Petersburg State University, 198504 Saint Petersburg, Russia
4 Departamento de Física de Materiales UPV/EHU, Centro de Física de Materiales CFM—MPC and Centro Mixto CSIC-UPV/EHU, 20080 San Sebastián/Donostia, Spain
5 Department of Applied Physics II, Faculty of Science and Technology, University of the Basque Country UPV/EHU, Apdo. 644, 48080 Bilbao, Spain
6 Institute of Strength Physics and Materials Science, Russian Academy of Sciences, 634021 Tomsk, Russia
7 Institut für Festkörperforschung and Institute for Advanced Simulation, Forschungszentrum Jülich and JARA, D-52425 Jülich, Germany
8 Max-Planck-Institut für Mikrostrukturphysik, Weinberg 2, D-06120 Halle, Germany
9 Institut für Theoretische Physik, Johannes Kepler Universität, A 4040 Linz, Austria

E-mail: mikhail.otrokov@gmail.com

Keywords: topological insulator, magnetic insulator, thin films, electronic structure, quantum anomalous Hall effect, topological magnetoelectric effect, density functional theory

Supplementary material for this article is available online

Abstract

An interplay of spin–orbit coupling and intrinsic magnetism is known to give rise to the quantum anomalous Hall and topological magnetoelectric effects under certain conditions. Their realization could open access to low power consumption electronics as well as many fundamental phenomena like image magnetic monopoles, Majorana fermions and others. Unfortunately, being realized very recently, these effects are only accessible at extremely low temperatures and the lack of appropriate materials that would enable the temperature increase is a most severe challenge. Here, we propose a novel material platform with unique combination of properties making it perfectly suitable for the realization of both effects at elevated temperatures. The key element of the computational material design is an extension of a topological insulator (TI) surface by a thin film of ferromagnetic insulator, which is both structurally and compositionally compatible with the TI. Following this proposal we suggest a variety of specific systems and discuss their numerous advantages, in particular wide band gaps with the Fermi level located in the gap.

1. Introduction

Chasing efficient ways to introduce time-reversal symmetry breaking perturbations in a topological insulator (TI) [1, 2] without using an external magnetic field represents nowadays a real challenge of research activity. The strong efforts in this direction are motivated by the possibility to realize the quantum anomalous Hall effect (QAHE) [3, 4], a quantized version of the AHE [5], and the topological magnetoelectric effect (TME) [4, 6, 7], where an electric field induces a topological contribution to the magnetization with a universal coefficient of proportionality quantized in units of $e^2/2h$. A key ingredient of the QAH state and TME, i.e. a time-reversal symmetry breaking, is achieved by virtue of a ferromagnetic (FM) order (in the most simple case—with an out-of-plane magnetization; although the QAH state can also be realized with an in-plane magnetization upon certain conditions [8–11]). FM order induces an exchange gap in the surface state of three-dimensional TI or an exchange splitting of the TI thin film gap edges (or those of a trivial insulator thin film). Then, owing to a spin–orbit coupling (SOC), an inversion of the band gap, formed by non-degenerate, spin polarized bands can arise. Further, the Fermi level should be tuned into the two-dimensional band gap removing by this any surface or bulk state contribution. By meeting all these conditions in a two-dimensional TI (or trivial insulator) thin film, one could realize the QAH state, in

which, unlike a quantum spin Hall state [12–14], only one pair of bands is inverted [15]. Characterized by a dissipationless edge mode carrying electrons of only one spin direction [3, 4], this unique effect represents a promising platform for creation of next-generation electronic devices as well as for incarnation of novel phenomena like Majorana fermions [2]. On the other hand, if the TI film is sufficiently thick to eliminate the finite-size effect [7, 16–18], the exactly quantized TME is expected to appear [4], its direct consequences being the image magnetic monopole and topological Kerr or Faraday rotation [2]. While the QAH state has already been observed [19–28] and lately found to show indications of TME in the $Cr_x(Bi_{1-y}Sb_y)_{2-x}Te_3$ thin films [29], the practical realization of the TME at a 3D TI surface without an external magnetic field still remains elusive, although highly desirable [7, 16–18]. So far the quantized magneto-optical effect has been observed only at the surface of a nonmagnetic TI under an external magnetic field [30, 31].

Nowadays, that is almost four years after its realization, the rising of the QAHE temperature above 2 K still represents a great challenge. The main obstacles seem to be the inhomogeneity of the topological state coupling to the doped-in magnetic moments and the presence of the parasitic conduction in the bulk-like region [25, 28]. The former is clearly illustrated by a recent scanning tunneling spectroscopy study of the single crystal $Cr_x(Bi_{1-y}Sb_y)_{2-x}Te_3$ surface, revealing that a random distribution of the magnetic dopants results in a fluctuation of the Dirac point (DP) gap size, varying roughly from 10 to 50 meV [32]. This diminishes the effective energy barrier for the carriers thermal activation that determines the temperature scale of the QAHE observation. Another possible factor contributing to the QAH state deterioration is an appearance of the dissipative conduction channels [25] due to metallization of the magnetically-doped TI bulk-like region.

Here, using first-principles calculations, we propose a new, simple and efficient method to incorporate magnetism in TI surfaces that permits to avoid problems caused by an inhomogeneous dopants distribution and/or possible metallization of the bulk-like region. Instead of a surface [33–35] or bulk doping [4, 32, 36], surface alloying [34, 37, 38] or magnetic proximity effect [39, 40], we use a *magnetic extension* of the TI surface (or a thin film) to achieve an efficient time-reversal symmetry breaking. Namely, taking advantage of the situation when the ferromagnetic and topological insulators have (i) exactly the same or an affine crystal structure and (ii) a similar atomic composition, we consider an FM insulator (FMI) film deposited on top of a TI surface. In this way, the absence of a sharp interface between the two subsystems, minimal differences in the atomic composition, and a perfect or a very good crystal lattice matching make the FMI film a natural extension of the TI. As a consequence, the topological surface state substantially relocates into the FMI film and acquires a giant DP gap (several tens of meV) due to a strong exchange interaction with 3*d* moments, occupying a complete atomic layer in the magnetically-extended region. This observation is supported by the highly accurate total-energy calculations revealing an FM order with an out-of-plane easy magnetization axis for a number of FMI/TI systems under consideration. Moreover, the approach proposed here offers other numerous advantages such as intrinsic Fermi level location inside the gap, highly-ordered crystal structure, absence of the harmful trivial surface or interface states, intactness of the TI bulk-like region, and, finally, a lot of possible combinations of magnetic and non-magnetic insulators. Altogether, these properties undoubtedly show that the magnetic extension is an extremely promising way towards enhancement of the QAHE observation temperature and eventual realization of the quantized TME at TI surfaces without an external magnetic field.

2. Results and discussion

2.1. Structure and magnetism

In the present work, we study systems consisting of tetradymite-type nonmagnetic semiconductor films of different thicknesses (including those corresponding to 3D and 2D TIs), sandwiched between two septuple-layer(SL)-thick films of a tetradymite-family magnetic insulator. Such a system design is experimentally feasible since the septuple or quintuple layers (QLs) of the tetradymite-type compounds are very stable units on their own due to the strong covalent-ionic type bonding between the atomic layers inside the block. The stability of such blocks is confirmed by a QL-by-QL epitaxial growth mode [41]. We note that the geometry described above allows realizing both QAHE and TME [18, 29]. Besides, the use of a thick TI slab allows visualizing the magnetic extension effect in a full measure, when the topological surface state splits due to magnetism. On the other hand, a small thickness of an FMI film ensures a near-surface location of the gapped topological state even if it does not significantly penetrate into the extended region. Therefore, our theoretical predictions can be verified experimentally by using a standard angle-resolved photoemission spectroscopy.

The starting point of our study is the fact that the family of the tetradymite-like compounds $XB^{VI}{\cdot}A^{V}_{2}B^{VI}_{3}$ (A^{V} = Sb, Bi; B^{VI} = Se, Te; *X* is, e.g. Ge, Sn or Pb) [42, 43] does not restrict itself to the nonmagnetic materials only. These compounds crystallize in a rhombohedral structure (space group $R\bar{3}m$ (166)), which is comprised of the SL building blocks stacked along the *c* axis and separated by a van der Waals gap. Importantly for our purposes, there exist quite a few stable XB^{VI} compounds with the hexagonal low-index surfaces, what makes them potentially compatible with those of the $A^{V}_{2}B^{VI}_{3}$ tetradymite family. Among them, in particular, there are magnetic semiconductors, an interesting representative

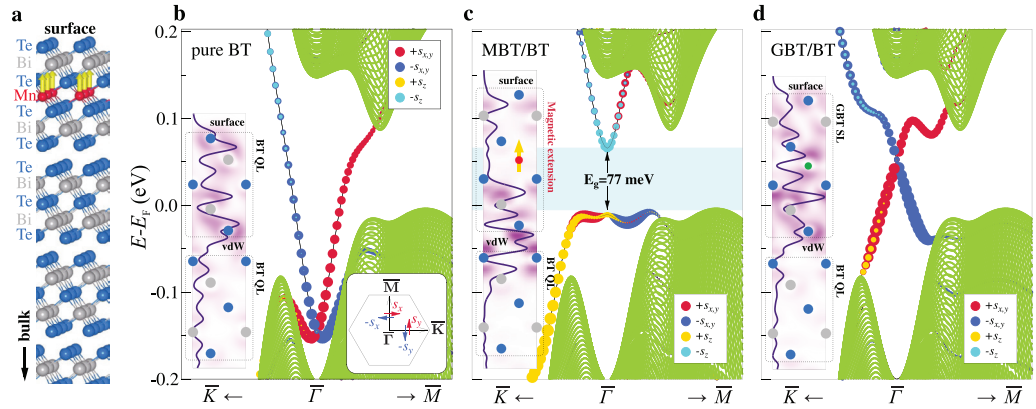

Figure 1. (a) Atomic structure of MBT/BT with gold arrows indicating the Mn 3*d* moments, pointing out of the surface plane. ((b)–(d)) Spin-resolved surface band spectra of BT (b), MBT/BT (c) and $GeBi_2Te_4$/BT (GBT/BT (d)). The size of color circles reflects the value and sign of the spin vector Cartesian projections, with red/blue colors corresponding to the positive/negative in-plane components (that directed perpendicular to the **k** vector), and gold/cyan reflecting the out-of-plane components $+s_z/-s_z$. Green areas correspond to the bulk band structure projected onto the surface Brillouin zone. The insets to (b)–(d) show the real space distribution of the topological surface state charge density as projected onto the *ac*-plane (color map in the white-to-pink palette) and as integrated over the *ab* plane (purple line) for BT, MBT/BT and GBT/BT, respectively. In the insets, the 'vdW' stays for the van der Waals gap.

being the room temperature antiferromagnet MnTe [44]. It is therefore quite logical to suggest the $MnB^{VI}_2A^{V}_2B^{VI}_3$ compounds with the tetradymite-like structure to be stable as well. Recently, this indeed has been confirmed by Lee *et al* [45] who reported a successful growth of the R$\bar{3}$m-group bulk $MnBi_2Te_4$ for the first time. The material was found to be a *p*-type semiconductor and its in-plane lattice constant was measured to be 4.334 Å, which matches very well to that of various tetradymite-type TIs like Bi_2Te_3, Sb_2Te_3 and others (see supplementary note 1 (stacks.iop.org/TDM/4/025082/mmedia)). Having the same or allied crystal structure, a very similar atomic composition and being well-lattice-matched, such $MnBi_2Te_4$/TI (MBT/TI) systems are expected to be readily grown by molecular-beam epitaxy. A natural question then arises: how will the topological surface state of a particular TI be changed upon a magnetic extension by an SL of $MnBi_2Te_4$?

Before answering this question, we first determine the magnetic ground state of the MBT/TI systems. As a substrate for an MBT film deposition, we take a thick film (6QL slab) of one of the most studied TIs—Bi_2Te_3 (BT), see figure 1(a). Our total energy density functional theory calculations reveal that MBT/BT is a ferromagnet with an out-of-plane easy axis, Curie temperature of 39 K, and a local moment of 4.613 μ_B per Mn atom (supplementary note 2).

2.2. Magnetically-extended TI surface for quantized magnetoelectric effect

We now study the surface band structure of the MBT/BT system. Figure 1(b) shows the topological state of Bi_2Te_3(0 0 0 1) with its DP located below the bulk valence band maximum [46]. The deposition of the MBT SL film on the BT surface leads to substantial changes in the low-energy spectrum. As it is seen in figure 1(c), the surface band structure of MBT/BT is fully gapped—the gap in the DP reaches a gigantic value of 77 meV and the Fermi level is located within it. Moreover, the surface band gap almost completely lies within the bulk one, despite the fact that the original DP of the pure BT surface is located ∼150 meV lower than the bulk valence band maximum. A clear explanation comes out if instead of the MBT/BT system the $[GeBi_2Te_4]_{1SL}/Bi_2Te_3$ (GBT/BT) one is considered. While the GBT-extension of the Bi_2Te_3 surface expectedly keeps the topological state gapless, it leads to a strong upward shift of the DP which turns out to be located in the fundamental band gap (figure 1(d)). A similar behaviour has recently been observed in the case of nonmagnetic TI-based heterostructures [47, 48] and has been shown to depend on the electron affinities and band gap widths of the substrate and overlayer materials. The mechanism behind the giant DP splitting is illustrated in the insets of figures 1(b)–(d), showing the real space distribution of the topological surface states of the respective cases. It can be seen, that the topological state largely relocates into the magnetically extended region where the time-reversal symmetry is broken owing to an out-of-plane magnetization of the Mn layer. Despite the wave function of the topological surface state does not show a maximum on Mn atoms, its localization in the MBT SL and on the Mn layer in particular turns out to be sufficient to induce a very large splitting at the DP. In the supplementary note 3, we show that the DP gaps up to 87 meV have been calculated for the MBT/BT system within the physically-meaningful range of the effective U_{eff} parameter values, taking into account a strongly-correlated nature of the Mn 3*d*-states. The ultimate value of this parameter and, therefore, the DP gap size can be determined from photoemission experiments that we hope to inspire.

The situation shown in figure 1(c) is in stark contrast with the case of well-defined interfaces, formed

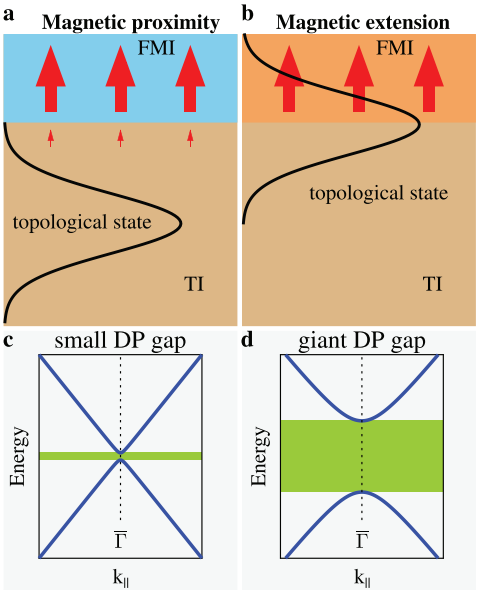

Figure 2. Schematic illustration of (a) the magnetic proximity effect following [39] and (b) the magnetic extension of the topological insulator surface. The effects respectively yield small (c) and giant (d) DP gaps. Large and small arrows in panels (a) and (b) denote local and induced magnetic moments, respectively.

between magnetic and topological insulators with different crystal structures, e.g. MnSe and Bi_2Se_3. As shown in [39], the Dirac cone of Bi_2Se_3, localized in the topmost QL in the free surface case, relocates to the underlying QL upon interfacing with MnSe, what results in a quite moderate DP splitting of 8.5 meV. Furthermore, because of substantial modification of the interface potential, a trivial interface state appears, making the spectrum gapless. In MBT/BT, the interface region is well comparable to the van der Waals region of the BT substrate and, therefore, the MBT/BT low-energy spectrum is essentially free of parasitic trivial bands at any **k**. Besides, the atomic composition of the layers, lying near the van der Waals gap, for the MBT and interfacial BT QL essentially coincides up to the third atomic layer inclusively, see figure 1(a). These factors altogether lead to a magnetic extension of the Bi_2Te_3 surface characterized by the absence of the trivial states and by the topological state that is largely localized in the magnetic block.

It is worth to highlight a fundamental difference between the magnetic extension approach that we propose and the magnetic proximity effect, that has previously been used to lift the time-reversal symmetry at the TI surface [39, 40] or create a QAH state in graphene [49, 50]. In the magnetic proximity effect, a magnetically ordered system induces finite magnetization in a nonmagnetic system through the interface coupling (figure 2(a)). The induced magnetization can lift band degeneracies in the nonmagnetic system: a small gap opens at the DP of a TI [39], see figure 2(c), or the Dirac cone of graphene experiences exchange splitting [49, 50]. In the magnetic extension approach the situation is completely different: the topological state

Table 1. Calculated values of the Dirac point band gaps for various systems.

System	E_g (meV)
$MnBi_2Te_4/Bi_2Te_3$	77
$MnBi_2Te_4/Sb_2Te_3$	73
$MnBi_2Te_4/Bi_2Te_2Se$	52
$MnBi_2Te_4/Bi_2Te_2S$	47
$MnSb_2Te_4/Sb_2Te_3$	25

significantly penetrates into the magnetic film region and strongly splits due to direct interaction with the magnetic moments of Mn atoms (figures 2(b) and (d)).

It is obvious from the above said that, due to its remarkable action on the topological state, magnetic extension appears to be a perfect approach for the quantized TME observation at the surfaces of thick TI films without magnetic field [18]. In table 1, one can find some more examples of the systems with the giant DP splittings up to 73 meV. The corresponding band structures are shown in the supplementary note 4. We envisage a hardly limited number of systems, which can be produced using the magnetic extension approach. This is possible owing to a great variety of the tetradymite-like TIs, consisting of different blocks and their combinations [42, 43], disordered TIs of the $Bi_{2-x}Sb_xTe_{3-y}Se_y(S_y)$ type, TIs beyond the tetradymite family [51], FMI/TI superstructures and, possibly, other FMIs.

2.3. Thin films limit and QAH phase

We have constructed various MBT/$[Bi_2Te_3]_{nQL}$/MBT heterostructures with different number of the BT QLs, $n = 1 - 5$. Figure 3 compares the band structures of the MBT/$[Bi_2Te_3]_{2QL}$/MBT sandwich calculated without and with spin–orbit coupling included. Note that the calculations have been done assuming the parallel alignment of magnetic moments of the MBT blocks separated by n QL(s) of Bi_2Te_3. Since the MBT SLs are almost magnetically decoupled, this can always be achieved using an external magnetic field, as it has been done in the recent experiments showing the highest QAH temperatures in modulation-doped TI films [25, 29] (see also [52] for a theoretical analysis of the modulation-doped QAH insulator). It can be seen in figures 3(a) and (b) that SOC causes an inversion of a pair of spin polarized bands in the $\overline{\Gamma}$-point vicinity, which is a prerequisite for the QAH state onset. Indeed, when spin–orbit coupling is absent (figure 3(a)), both the upper and lower gap edges are formed by a pair of bands of opposite spins near the Brillouin zone center. However, with SOC included, both upper valence bands (lower conduction bands) feature the majority (minority) spins $+s_z$ ($-s_z$) around the $\overline{\Gamma}$-point. In other words, one of the two upper valence bands (lower conduction bands) changes its spin on the opposite near $k_\parallel = 0$ owing to spin–orbit coupling, what can be recognized by a change of the line's color in figures 3(a) and (b). To confirm the nontriviality

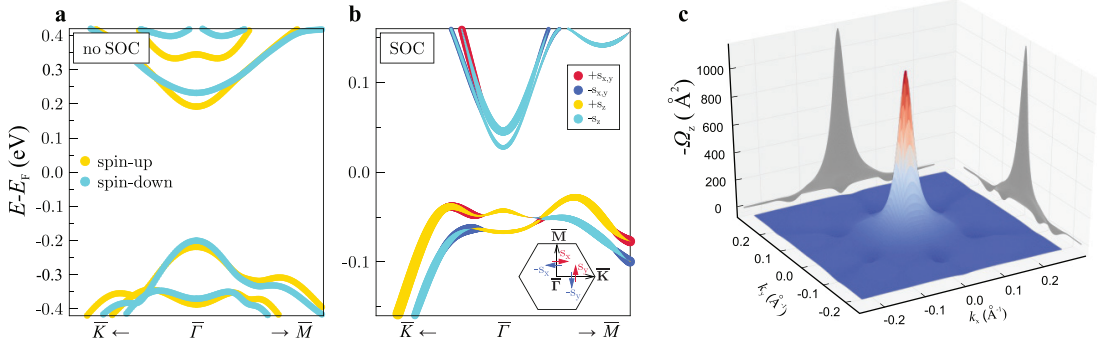

Figure 3. (a) and (b) Spin-resolved band structures of MBT/$[Bi_2Te_3]_{2QL}$/MBT, calculated without and with SOC, respectively. The color coding is the same as in figure 1. (c) Berry curvature calculated for MBT/$[Bi_2Te_3]_{2QL}$/MBT.

Table 2. Calculated band gaps for various QAH insulators.

System	E_g (meV)
MBT/$[Bi_2Te_3]_{1QL}$/MBT	38
MBT/$[Bi_2Te_3]_{2QL}$/MBT	56
MBT/$[Bi_2Te_3]_{3QL}$/MBT	56
MBT/$[Bi_2Te_3]_{4QL}$/MBT	60
MBT/$[Bi_2Te_3]_{5QL}$/MBT	61
MBT/$[SnSb_2Te_4]_{1SL}$/MBT	40
MBT/$[SnSb_2Te_4]_{2SL}$/MBT	16
MBT/$[PbSb_2Te_4]_{1SL}$/MBT	55
MBT/$[PbSb_2Te_4]_{2SL}$/MBT	55

of the MBT/$[Bi_2Te_3]_{2QL}$/MBT band structure in a more solid way, the Chern number calculations have been performed. Using an *ab initio*-based tight-binding approach (see methods section), a non-zero Berry curvature has been found near the $\bar{\Gamma}$-point (figure 3(c)) yielding a Chern number of -1 upon integration over the first Brillouin zone. This result has been reproduced by an independent calculation of the Chern number with the Z2Pack thus confirming the QAH state in MBT/$[Bi_2Te_3]_{2QL}$/MBT with a band gap of 56 meV. The equality of the Chern number C to -1 for MBT/$[Bi_2Te_3]_{2QL}$/MBT means that there will be a single dissipationless chiral edge mode at any border of the film. The Hall conductance facilitated by the edge mode is related to the Chern number as $\sigma_{xy} = Ce^2/h$ and is therefore quantized to a value of $-e^2/h$ for the proposed system. Following the above-described strategy, we have found a number of QAH insulators with the Chern number equal to -1 and the band gaps ranging from 16 to 61 meV (table 2 and supplementary note 5).

3. Outlook and conclusions

The above-described properties reveal that the magnetic extension is an extremely promising way of the time-reversal symmetry breaking in TIs. In the supplementary note 6 we give an extensive comparison to other approaches of the time-reversal symmetry breaking in TIs [32, 33, 37, 39] as well as to specific QAH systems (both synthesized [20–29] and theoretically-proposed [15, 53–69]) that is summarized here as follows. First, in comparison to the strongly-disordered $(V_x)Cr_x(Bi_{1-y}Sb_y)_{2-x}Te_3$ QAH insulators studied in the experiments [20–29], the MBT/TI/MBT sandwiches yield up to at least six times larger band gaps and are expected to show a highly-ordered structure, inherent of stoichiometric materials. The latter makes the magnetic extension based systems stable against the in-gap dopant states [70] as well as possible superparamagnetic behavior [26, 27]. We speculate that an increase of nearly one order of magnitude of the QAHE observation temperature may be expected owing to these advances. Second, having considered a variety of theoretical proposals of the QAH insulators beyond those of the tetradymite family [15, 53–68], one can conclude that the QAH insulators based on the magnetic extension approach proposed appear nowadays as an optimal platform for the QAHE. Indeed, while the techniques for a controllable growth of the wide band gap honeycomb-structure QAH insulators [57, 60] are still to be elaborated, the magnetic-extension-based QAH insulators can be implemented immediately making use of existing advanced technology of the tetradymite-type compounds epitaxial growth. Finally, the magnetic extension approach is expected to partly circumvent the difficulty coming from the constraint on the photon frequency $\omega \ll E_g/\hbar$ [4] (E_g is the DP gap), that requires wide gap materials for an accurate measurement of the topological Kerr and Faraday rotations (see supplementary note 6). We stress that among the experimentally-feasible specific proposals, magnetically-extended TI surfaces feature largest DP gaps, what makes them best candidates for realization of the quantized TME at TI surfaces at zero magnetic field.

Thus, using *ab initio* band structure calculations, we have proposed a magnetic extension of topological insulator surfaces—a novel approach for the time-reversal symmetry breaking. The key idea behind it, is the use of topological and magnetic insulators of the allied crystal structure and similar atomic composition, such that the surface features of the former are naturally extended upon the deposition of the latter. In this case, the topological surface state does not meet any

significant interfacial potential and largely penetrates into the magnetically-extended part getting gigantically split, once the ferromagnetic state with an out-of-plane magnetization onsets there. Moreover, in such systems, the Fermi level is intrinsically located within the induced Dirac point gap, while trivial surface or interface states are essentially absent in the low-energy spectrum. Importantly, the approach relies on the use of the stoichiometric magnetic compounds thus ruling out possible disorder-related effects. Such a combination of properties renders the magnetically-extended topological insulator surface to be a unique system, perfectly suitable for the eventual experimental observation of the topological magnetoelectric effect at TI surfaces without magnetic field, as well as for the realization of the quantum anomalous Hall state significantly beyond temperatures reached to date.

4. Methods

Electronic structure calculations were carried out within the density functional theory using the projector augmented-wave method [71] as implemented in the VASP code [72, 73]. The exchange-correlation energy was treated using the generalized gradient approximation [74]. The Hamiltonian contained the scalar relativistic corrections and the spin–orbit coupling was taken into account by the second variation method [75]. In order to describe the van der Waals interactions we made use of the DFT-D2 [76] and the DFT-D3 [77, 78] approaches, giving similar results. The energy cutoff for the plane-wave expansion was set to 270 eV. The Mn 3*d*-states were treated employing the GGA + *U* approach [79] within the Dudarev scheme [80]. Taking into account that the Mn layer local environment in MBT is the same as that in bulk MnTe, the $U_{\mathrm{eff}} = U - J$ value for the Mn 3*d*-states was chosen to be the same as the one estimated for the bulk MnTe case [81], i.e. 5.34 eV. Nevertheless, an extensive testing was performed for the MBT/BT system in order to ensure stability of the results against the U_{eff} value (see supplementary note 3). It was found that the magnetic ordering and magnetic anisotropy do not change qualitatively when the U_{eff} value changes from 3 to 5.34 eV.

The magnetically-extended TI surfaces were simulated within a model of repeating slabs separated by a vacuum gap of a minimum of 10 Å. The FMI films were symmetrically attached to both sides of the substrate slab to preserve the inversion symmetry, which was maintained for the magnetically-ordered cases as well. Our total-energy calculations show, that the lateral location of the FMI SL that maintains the ...*ABCABCABC*... stacking of the substrate layers is the most favorable one. Therefore all calculations have been performed for this type of connection between the substrate and FMI film. The thicknesses of the TI substrates chosen were such that the maximal hybridization gap in the DP did not exceed 1 meV. These were the 6 QL and 7 SL slabs for the $A_2^{V}B_3^{VI}$ and $A^{IV}B^{VI}{\cdot}A_2^{V}B_3^{VI}$ TIs, respectively. The in-plane lattice parameters of the magnetically-extended TIs were fixed to the experimental ones of corresponding TIs, while the interlayer distances were optimized for the two upper structural blocks using a conjugate-gradient algorithm and a force tolerance criterion for convergence of 0.03 eV $\mathrm{Å}^{-1}$ (spin–orbit coupling was included during the relaxation). Relaxations and electronic structure calculations were performed using a $\overline{\Gamma}$-centered *k*-point grid of $11 \times 11 \times 1$ in the two-dimensional Brillouin zone.

To model the FM and collinear AFM phases, the $(1 \times \sqrt{3})$ rectangular in-plane supercells containing two atoms per atomic layer were constructed for each system under consideration. For the verification of the MBT/BT FM state stability against the non-collinear AFM state formation the $(\sqrt{3} \times \sqrt{3})R30°$ in-plane supercells containing three atoms per atomic layer were used. Both $(1 \times \sqrt{3})$ and $(\sqrt{3} \times \sqrt{3})R30°$ in-plane cells as well as the magnetic structures mentioned are visualized in the supplementary note 2. In all these calculations, the slab thicknesses were maintained the same as for the surface band structure calculations. For the total-energy calculations, the two-dimensional Brillouin zones were sampled by the $9 \times 5 \times 1$ and $5 \times 5 \times 1$ $\overline{\Gamma}$-centered *k*-point grids in the cases of $(1 \times \sqrt{3})$ and $(\sqrt{3} \times \sqrt{3})R30°$ in-plane cells, respectively.

For the calculation of the band contribution to the magnetic anisotropy energy, E_b, the *k*-mesh of $25 \times 25 \times 1$ was chosen after the convergence tests performed (see supplementary note 7). The calculations were done for the thicknesses of 44 and 56 atomic layers for the magnetically-extended surfaces of the QL- and SL-based TIs, respectively. To calculate E_b, the energies for three inequivalent magnetization directions—Cartesian *x*, *y* (in-plane) and *z* (out-of-plane)—were calculated and E_b was determined as the difference $E_{\mathrm{in-plane}}$—E_z, where the $E_{\mathrm{in-plane}}$ is the energy of the most energetically favorable in-plane direction of magnetization. The energy convergence criterion was set to 10^{-7} eV providing a well-converged E_b (the values of the order of few tenth of meV) while excluding 'accidental' convergence. The cutoff radius of a minimum of 20 microns was used to calculate dipole-dipole contribution, E_d, to the magnetic anisotropy energy, E_a.

Exchange coupling parameters of the $MnBi_2Te_4$ SL were calculated using the Korringa–Kohn–Rostoker method within a full potential approximation to the crystal potential [82]. We took an angular momentum cutoff of $l_{\mathrm{max}} = 3$ for the Green's function and a k-point mesh of $25 \times 25 \times 1$ for the 2D Brillouin zone integration.

The Chern numbers have been independently calculated using Z2Pack [83, 84] and *ab initio*-based tight-binding calculations within the WANNIER90 interface to the VASP [85, 86]. In the latter case, using a tight-binding Hamiltonian *H* in the Wannier function basis, the Berry curvature tensor has been calculated applying Kubo formula [87, 88]:

$$\Omega_{n,\alpha\beta}(\mathbf{k}) = -\mathrm{Im}\sum_{v\neq n}\frac{\langle n|\nabla_\alpha H(\mathbf{k})|v\rangle\langle v|\nabla_\beta H(\mathbf{k})|n\rangle}{(E_n(\mathbf{k})-E_v(\mathbf{k}))^2}, \quad (1)$$

where $\nabla_\alpha H$ is a velocity operator, while $|n\rangle$ and $|v\rangle$ are the Bloch states for each $\mathbf{k}$ with energies $E_n(\mathbf{k})$ and $E_v(\mathbf{k})$, respectively. Total Berry curvature has been obtained by summation over the occupied states $\Omega_{\alpha\beta}(\mathbf{k}) = \sum_n f_n \Omega_{n,\alpha\beta}(\mathbf{k})$, f_n being the Fermi–Dirac distribution. Three components of the 'magnetic' gauge field are obtained using $\Omega_\gamma(\mathbf{k}) = \epsilon_{\alpha\beta\gamma}\Omega_{\alpha\beta}(\mathbf{k})$. Here $\epsilon_{\alpha\beta\gamma}$ is a three-component antisymmetric Levi–Civita tensor. Chern number is evaluated as a Berry gauge flux over the 2D Brillouin zone, $C = 1/(2\pi)\int_S \Omega_z(\mathbf{k})\mathrm{d}k^2$, where S is the 2D Brillouin zone area and $\Omega_z(\mathbf{k})$—a normal component of the Berry curvature.

Acknowledgments

MMO acknowledges useful discussions with SV Eremeev. We acknowledge support by the University of the Basque Country (Grant Nos. GIC07IT36607 and IT-756-13), the Spanish Ministry of Science and Innovation (Grant Nos. FIS2013-48286-C02-02-P, FIS2013-48286-C02-01-P, and FIS2016-75862-P) and Tomsk State University Academic DI Mendeleev Fund Program in 2015 (research grant N 8.1.05.2015). Partial support by the Saint Petersburg State University project No. 15.61.202.2015 is also acknowledged. AE acknowledges financial support from DFG through priority program SPP1666 (Topological Insulators). The calculations were performed in the Donostia International Physics Center and Resource Center 'Computer Center of SPbU' (http://cc.spbu.ru).

References

[1] Hasan M Z and Kane C L 2010 *Rev. Mod. Phys.* **82** 3045–67
[2] Qi X L and Zhang S C 2011 *Rev. Mod. Phys.* **83** 1057–110
[3] Qi X L, Wu Y S and Zhang S C 2006 *Phys. Rev.* B **74** 085308
[4] Qi X L, Hughes T L and Zhang S C 2008 *Phys. Rev.* B **78** 195424
[5] Onoda M and Nagaosa N 2003 *Phys. Rev. Lett.* **90** 206601
[6] Essin A M, Moore J E and Vanderbilt D 2009 *Phys. Rev. Lett.* **102** 146805
[7] Tse W K and MacDonald A H 2010 *Phys. Rev. Lett.* **105** 057401
[8] Zhang Y and Zhang C 2011 *Phys. Rev.* B **84** 085123
[9] Liu X, Hsu H C and Liu C X 2013 *Phys. Rev. Lett.* **111** 086802
[10] Ren Y, Zeng J, Deng X, Yang F, Pan H and Qiao Z 2016 *Phys. Rev.* B **94** 085411
[11] Sheng X L and Nikolic B K 2016 arXiv:1610.02719
[12] Kane C L and Mele E J 2005 *Phys. Rev. Lett.* **95** 146802
[13] Murakami S 2006 *Phys. Rev. Lett.* **97** 236805
[14] Bernevig B A, Hughes T L and Zhang S C 2006 *Science* **314** 1757–61
[15] Liu C X, Qi X L, Dai X, Fang Z and Zhang S C 2008 *Phys. Rev. Lett.* **101** 146802
[16] Qi X L, Li R, Zang J and Zhang S C 2009 *Science* **323** 1184–7
[17] Nomura K and Nagaosa N 2011 *Phys. Rev. Lett.* **106** 166802
[18] Wang J, Lian B, Qi X L and Zhang S C 2015 *Phys. Rev.* B **92** 081107
[19] Chang C Z *et al* 2013 *Science* **340** 167–70
[20] Checkelsky J G, Yoshimi R, Tsukazaki A, Takahashi K S, Kozuka Y, Falson J, Kawasaki M and Tokura Y 2014 *Nat. Phys.* **10** 731–6
[21] Kou X *et al* 2014 *Phys. Rev. Lett.* **113** 137201
[22] Chang C Z, Zhao W, Kim D Y, Zhang H, Assaf B A, Heiman D, Zhang S C, Liu C, Chan M H and Moodera J S 2015 *Nat. Mater.* **14** 473–7
[23] Kou X *et al* 2015 *Nat. Commun.* **6** 8474
[24] Feng Y *et al* 2015 *Phys. Rev. Lett.* **115** 126801
[25] Mogi M, Yoshimi R, Tsukazaki A, Yasuda K, Kozuka Y, Takahashi K S, Kawasaki M and Tokura Y 2015 *Appl. Phys. Lett.* **107** 182401
[26] Lachman E O *et al* 2015 *Sci. Adv.* **1** e1500740
[27] Grauer S, Schreyeck S, Winnerlein M, Brunner K, Gould C and Molenkamp L W 2015 *Phys. Rev.* B **92** 201304
[28] Chang C Z, Zhao W, Li J, Jain J K, Liu C, Moodera J S and Chan M H W 2016 *Phys. Rev. Lett.* **117** 126802
[29] Okada K N, Takahashi Y, Mogi M, Yoshimi R, Tsukazaki A, Takahashi K S, Ogawa N, Kawasaki M and Tokura Y 2016 *Nat. Commun.* **7** 12245
[30] Wu L, Salehi M, Koirala N, Moon J, Oh S and Armitage N 2016 *Science* **354** 1124–7
[31] Dziom V *et al* 2016 arXiv:1603.05482
[32] Lee I *et al* 2015 *Proc. Natl Acad. Sci.* **112** 1316–21
[33] Liu Q, Liu C X, Xu C, Qi X L and Zhang S C 2009 *Phys. Rev. Lett.* **102** 156603
[34] Schlenk T *et al* 2013 *Phys. Rev. Lett.* **110** 126804
[35] Otrokov M M, Chulkov E V and Arnau A 2015 *Phys. Rev.* B **92** 165309
[36] Vergniory M G *et al* 2014 *Phys. Rev.* B **89** 165202
[37] Henk J, Flieger M, Maznichenko I V, Mertig I, Ernst A, Eremeev S V and Chulkov E V 2012 *Phys. Rev. Lett.* **109** 076801
[38] Polyakov A *et al* 2015 *Phys. Rev.* B **92** 045423
[39] Eremeev S V, Men'shov V N, Tugushev V V, Echenique P M and Chulkov E V 2013 *Phys. Rev.* B **88** 144430
[40] Katmis F *et al* 2016 *Nature* **533** 513
[41] Zhang Y *et al* 2010 *Nat. Phys.* **6** 584–8
[42] Eremeev S V *et al* 2012 *Nat. Commun.* **3** 635
[43] Silkin I V, Menshchikova T V, Otrokov M M, Eremeev S V, Koroteev Y M, Vergniory M G, Kuznetsov V M and Chulkov E V 2012 *JETP Lett.* **96** 322–5
[44] Podgorny M and Oleszkiewicz J 1983 *J. Phys. C: Solid State Phys.* **16** 2547
[45] Lee D S, Kim T H, Park C H, Chung C Y, Lim Y S, Seo W S and Park H H 2013 *CrystEngComm* **15** 5532–8
[46] Sessi P, Otrokov M M, Bathon T, Vergniory M G, Tsirkin S S, Kokh K A, Tereshchenko O E, Chulkov E V and Bode M 2013 *Phys. Rev.* B **88** 161407
[47] Menshchikova T V, Otrokov M M, Tsirkin S S, Samorokov D A, Bebneva V V, Ernst A, Kuznetsov V M and Chulkov E V 2013 *Nano Lett.* **13** 6064–69
[48] Men'shov V N, Tugushev V V, Menshchikova T V, Eremeev S V, Echenique P M and Chulkov E V 2014 *J. Phys.: Condens. Matter* **26** 485003
[49] Qiao Z, Ren W, Chen H, Bellaiche L, Zhang Z, MacDonald A and Niu Q 2014 *Phys. Rev. Lett.* **112** 116404
[50] Zhang J, Zhao B, Yao Y and Yang Z 2015 *Sci. Rep.* **5** 10629
[51] Kuroda K *et al* 2010 *Phys. Rev. Lett.* **105** 146801
[52] Menshov V N, Tugushev V V and Chulkov E V 2016 *JETP Lett.* **104** 453–9
[53] Xu G, Weng H, Wang Z, Dai X and Fang Z 2011 *Phys. Rev. Lett.* **107** 186806
[54] Zhang H, Lazo C, Blügel S, Heinze S and Mokrousov Y 2012 *Phys. Rev. Lett.* **108** 056802
[55] Wang Z F, Liu Z and Liu F 2013 *Phys. Rev. Lett.* **110** 196801
[56] Zhang X L, Liu L F and Liu W M 2013 *Sci. Rep.* **3** 2908
[57] Garrity K F and Vanderbilt D 2013 *Phys. Rev. Lett.* **110** 116802
[58] Garrity K F and Vanderbilt D 2014 *Phys. Rev.* B **90** 121103
[59] Wang Q Z, Liu X, Zhang H J, Samarth N, Zhang S C and Liu C X 2014 *Phys. Rev. Lett.* **113** 147201
[60] Wu S C, Shan G and Yan B 2014 *Phys. Rev. Lett.* **113** 256401
[61] Zhang H, Wang J, Xu G, Xu Y and Zhang S C 2014 *Phys. Rev. Lett.* **112** 096804
[62] Jin K H and Jhi S H 2015 *Sci. Rep.* **5** 8426
[63] Zhou T, Zhang J, Zhao B, Zhang H and Yang Z 2015 *Nano Lett.* **15** 5149–55

[64] Liu C C, Zhou J J and Yao Y 2015 *Phys. Rev.* B **91** 165430
[65] Xu G, Wang J, Felser C, Qi X L and Zhang S C 2015 *Nano Lett.* **15** 2019–23
[66] Xu G, Lian B and Zhang S C 2015 *Phys. Rev. Lett.* **115** 186802
[67] Dong L, Kim Y, Er D, Rappe A M and Shenoy V B 2016 *Phys. Rev. Lett.* **116** 096601
[68] Chen S P, Huang Z Q, Crisostomo C P, Hsu C H, Chuang F C, Lin H and Bansil A 2016 *Sci. Rep.* **6** 31317
[69] Wu M *et al* 2017 *2D Mater.* **4** 015015
[70] Sánchez-Barriga J *et al* 2016 *Nat. Commun.* **7** 10559
[71] Blöchl P E 1994 *Phys. Rev.* B **50** 17953–79
[72] Kresse G and Furthmüller J 1996 *Phys. Rev.* B **54** 11169–86
[73] Kresse G and Joubert D 1999 *Phys. Rev.* B **59** 1758–75
[74] Perdew J P, Burke K and Ernzerhof M 1996 *Phys. Rev. Lett.* **77** 3865–8
[75] Koelling D D and Harmon B N 1977 *J. Phys. C: Solid State Phys.* **10** 3107
[76] Grimme S 2006 *J. Comput. Chem.* **27** 1787–99
[77] Grimme S, Antony J, Ehrlich S and Krieg H 2010 *J. Chem. Phys.* **132** 154104
[78] Grimme S, Ehrlich S and Goerigk L 2011 *J. Comput. Chem.* **32** 1456–65
[79] Anisimov V I, Zaanen J and Andersen O K 1991 *Phys. Rev.* B **44** 943–54
[80] Dudarev S L, Botton G A, Savrasov S Y, Humphreys C J and Sutton A P 1998 *Phys. Rev.* B **57** 1505–9
[81] Youn S 2005 *J. Magn.* **10** 71–5
[82] Geilhufe M, Achilles S, Kbis M A, Arnold M, Mertig I, Hergert W and Ernst A 2015 *J. Phys.: Condens. Matter* **27** 435202
[83] Soluyanov A A and Vanderbilt D 2011 *Phys. Rev.* B **83** 235401
[84] Gresch D, Autes G, Yazyev O V, Troyer M, Vanderbilt D, Bernevig B A and Soluyanov A A 2017 *Phys. Rev.* B **95** 075146
[85] Marzari N and Vanderbilt D 1997 *Phys. Rev.* B **56** 12847–65
[86] Mostofi A A, Yates J R, Lee Y S, Souza I, Vanderbilt D and Marzari N 2008 *Comput. Phys. Commun.* **178** 685–99
[87] Thouless D J, Kohmoto M, Nightingale M P and den Nijs M 1982 *Phys. Rev. Lett.* **49** 405–8
[88] Yao Y, Kleinman L, MacDonald A H, Sinova J, Jungwirth T, Wang D S, Wang E and Niu Q 2004 *Phys. Rev. Lett.* **92** 037204